Constraint-Based Planning and Control of a Differential-Drive Robot for Navigation in Cluttered Environments

Zemerart Asani[1,2,3], Mohayad Omer[1,3], Bitlan Gheorghe[1,2], Mahaudens Aaron[1,2], Ouassim Benhamouche[2], Bram Vanderborght[1,3], Emanuele Garone[2], and Greet Van de Perre[1,3]

[1]Brussels Human Robotic Research Center (BruBotics), Vrije Universiteit Brussel, 1050 Brussels, Belgium.
[2]Service d'Automatique et d'Analyse des Systèmes (SAAS), Université libre de Bruxelles, 1050 Brussels, Belgium.
[3]Interuniversity Microelectronics Institute (IMEC), Leuven, Belgium.

zemerart.asani@vub.be, mohayad.abdelmonim.mahmoud.omer@vub.be

Abstract -
Mobile robots deployed in cluttered environments like in construction must navigate safely in cluttered spaces while satisfying state, input, and collision-avoidance constraints. Global path planners can generate optimal paths but do not guarantee safe execution, whereas constrained control methods ensure safety but often suffer from local minima. This paper proposes a hierarchical navigation framework that combines a fast Visibility-based Euclidean Shortest Path (VESHP) planner with an Explicit Reference Governor (ERG) for real-time constrained control. The VESHP planner computes a globally shortest collision-free path, while the ERG enforces constraints during execution without online optimization. Simulation and experimental results on a differential-drive mobile robot demonstrate safe, efficient navigation in highly cluttered construction environments.

Keywords -
Constrained control; Navigation; Obstacle avoidance.

Figure 1. Mobile robot avoiding obstacles. The initial position is denoted by P_1. While P_2, and P_3 are intermediate locations toward reaching the goal.

1 Introduction

The construction industry is one of the most economically important sectors worldwide, yet it continues to lag behind manufacturing and logistics in productivity and automation [1]. Increasing productivity requires the automation of repetitive and labor-intensive on-site operations through the integration of robotic systems [1, 2].

Recently, several robotic solutions for various construction tasks have been proposed to improve both efficiency and safety challenges in construction environments [3]. For instance, for robotic construction of walls a bricklaying robotic system is proposed [1, 4], [5]. This system is composed of a mobile manipulator and a crane that in coordination lay heavy blocks on a wall. In [6] a platform for safety inspections in hazardous areas is developed. Navigation and transportation in construction environment using hallway exploration inspired guidance approach is proposed in [7]. A robot for construction cleaning is proposed in [8], where a path-planning coverage algorithm has been proposed.

Many of these tasks require robots that can perform global motions throughout the environment, either to reach distant points, follow a path, or position precisely in the construction environment. As a result, mobile robots are increasingly being deployed on construction sites [9]. However, for practical on-site deployment, robots must guarantee safety, accuracy, and efficiency while navigating through highly cluttered environments [3].

In the navigation literature, motion planning algorithms are commonly categorized into *local* and *global* planners. Local planners (e.g., APF and DWA) enable real-time obstacle avoidance but may suffer from local minima. Global planners (e.g., A* and RRT) generate collision-free paths when a map is available. In visibility-graph approaches, graph construction is typically performed using ray casting or rotational sweep, followed by shortest-path search (e.g., A*). However, feasibility during execution depends on the robot controller [3].

These methods typically have high computational cost. In our previous work, a fast visibility-graph-based planner (VESHP) was proposed to compute shortest paths using precomputed visibility polygons [10], reducing graph construction cost and enabling faster online computation.

While the VESHP visibility-graph planning method provides globally optimal paths, safely executing such paths based solely on a pre-planned trajectory is challenging in practice. In real-world construction environments, mobile robots must continuously satisfy state, input, and collision-avoidance constraints during motion, which necessitates enforcing these requirements also at the control level rather than relying exclusively on high-level planning [11]. Constraint enforcement can be addressed using Model Predictive Control (MPC) or Reference Governor (RG) schemes. MPC provides systematic constraint handling but is computationally demanding due to online optimization [12], whereas ERG does not require online optimization, making it suitable for real-time implementation [11]. However, as pointed out in [11, 13] both may suffer from local minima in complex scenes with multiple obstacles.

To address these limitations, this work proposes a framework combining a fast global shortest-path planner with a constraint-aware control layer. The trajectory-based ERG is adapted for mobile robots to enforce state, input, and collision-avoidance constraints in real time. In addition, the VESHP planner is extended to account for the robot's dimensions while preserving shortest paths and guiding the ERG to avoid local minima. The resulting framework enables fast replanning through VESHP and efficient constraint enforcement through ERG, avoiding online optimization and remaining computationally lightweight compared to other hierarchical navigation stacks.

Through numerical simulations and real-world experiments, we demonstrate that the proposed framework enables efficient and safe mobile robot navigation in highly cluttered construction environments.

1.1 Notations

Throughout this paper, bold lowercase letters (e.g., $\boldsymbol{v}$) denote vectors, bold uppercase letters (e.g., $\boldsymbol{M}$) denote matrices, italic letters (e.g., t, m, L) denote scalars, and calligraphic letters (e.g., $\mathcal{S}, \mathcal{W}$) denote frames and sets. Round brackets indicate functional dependencies (e.g., $\boldsymbol{x}(s, \theta), \boldsymbol{x}(t)$). Square brackets denote concatenation (e.g., $\boldsymbol{v}_{i:k} = [\boldsymbol{v}_i^T, \ldots, \boldsymbol{v}_k^T]^T$) or element extraction (e.g., $\boldsymbol{v}[i : j]$). For a single element, we write $\boldsymbol{v}[i]$ or equivalently $\boldsymbol{v}_i$. An ordered collection of elements is denoted as a *sequence*. Given elements $s_1, \ldots, s_N, N \in \mathbb{N}$, the notation $(s_i)_{i=1}^N$ is used as shorthand for the sequence $(s_1, \ldots, s_N)$, while $\{s_i\}_{i=1}^N$ denotes the corresponding set $\{s_1, \ldots, s_N\}$. Any operation applied to $(\cdot)$ or $\{\cdot\}$ is understood element-wise. For a set $A \subset \mathbb{R}^2$, its interior is denoted by $\mathrm{int}(A)$.

2 Problem formulation

Consider a two-dimensional workspace $\mathcal{R} \subset \mathbb{R}^2$ in which a mobile robot operates. The environment contains a finite set of static obstacles $\{\mathcal{O}^i\}_{i=1}^N \subset \mathcal{R}$, where each obstacle $\mathcal{O}^i$ is a compact convex set. The free space is defined as

$$\overline{\mathcal{R}} := \mathcal{R} \setminus \bigcup_{j=1}^{N} \mathrm{int}\left(\mathcal{O}^j\right). \tag{1}$$

For the purpose of global path planning, each obstacle $\mathcal{O}^i$ is associated with a polygonal outer approximation $\tilde{\mathcal{O}}^i$ such that

$$\mathcal{O}^i \subseteq \tilde{\mathcal{O}}^i, \quad \forall i \in \{1, \ldots, N\}. \tag{2}$$

The goal of this paper is to address the following problem:

Problem 1. *Given an initial position $p_0 \in \tilde{\mathcal{R}}$ and a goal position $p_g \in \tilde{\mathcal{R}}$, compute a globally shortest collision-free path in the polygonal free space $\tilde{\mathcal{R}}$, using the VESHP visibility-graph planning method. Then, execute the computed path safely on the robot while considering its the nonlinear model of the mobile robot using the ERG constrained control scheme, ensuring real-time satisfaction of state, input, and collision-avoidance constraints during motion.*

In this paper, the following assumptions are considered.

Assumption 1. *The mobile robot operates in a flat planar workspace $\mathcal{R} \subset \mathbb{R}^2$.*

Assumption 2. *All obstacles in the environment are static and a priori known. For global planning purposes, obstacles are represented using polygonal approximations, while their exact geometric models are used for constraint enforcement during execution.*

3 Global motion planning

As a global shortest-path planning algorithm, we consider the recently proposed visibility-based Euclidean shortest path (VESHP) computation method based on precomputed visibility polygons [10]. This approach exploits the polygonal representation of the environment to compute an admissible shortest path from the initial point x_0 to the final point x_f, entirely contained in the free space $\overline{\mathcal{R}}$.

Formally, a path defined by the sequence of waypoints $(x_i)_{i=1}^M$ is admissible if

$$\begin{aligned} &\nexists \lambda : \lambda x_i + (1 - \lambda) x_{i+1} \notin \overline{\mathcal{R}}, \quad \forall i \in \{1, \ldots, M-1\}, \\ &\lambda \in [0, 1]. \end{aligned} \tag{3}$$

Among all admissible paths connecting x_0 and x_f, the VESHP algorithm computes the one minimizing the total Euclidean length $\sum_{i=1}^{M-1} \|x_{i+1} - x_i\|$.

The VESHP algorithm exploits the static nature of the environment to reduce the computational burden of shortest-path planning. In particular, since obstacles are assumed to be static, only the connections between the initial and final positions and the rest of the visibility graph need to be updated online. This leads to a decomposition of the visibility graph into two components:

i) a *static sub-graph*, encoding the visibility relationships among obstacle vertices and computed offline, and ii) a *dynamic sub-graph*, which connects the initial and goal positions to the static structure. The dynamic connections are efficiently determined using a geometric construction based on visibility polygons, while a subdivision of the environment into sub-regions further reduces the online search space.

Classical algorithms such as $A^\star$ and Dijkstra operate on a precomputed graph, whereas VESHP reduces the graph in the dynamic phase. As a result, VESHP enables fast computation of globally optimal paths by avoiding reconstruction of the full visibility graph when a new target is requested. Details can be found in [10], where the method reduces online computation time by one order of magnitude compared to rotational sweep line and by two orders compared to ray casting.

Unlike [10], which considers a point mobile agent, this work extends the applicability of the VESHP framework to robots with finite dimensions by inflating the environment accordingly. The VESHP algorithm is then applied unchanged in this inflated space, thereby preserving both admissibility and global optimality of the resulting path.

4 Constrained control

The control objective is to steer the mobile robot towards a sequence of reference goal points computed by the VESHP algorithm while ensuring satisfaction of state, input, and collision-avoidance constraints. The global planner provides a finite sequence of discrete waypoints, without imposing any time-parameterized trajectory between them.

A waypoint selector passes one waypoint at a time to the ERG, which treats it as as a local goal, and the motion between successive waypoints is autonomously generated by the constrained control layer while enforcing the constraints. The overall planning and control framework is illustrated in Figure 2.

For the mobile system, the following constraints are considered.

- Constraints on the operation region:

$$\boldsymbol{p}_{\min} \leq \boldsymbol{p} \leq \boldsymbol{p}_{\max}. \tag{4}$$

- Constraints on the input:

$$\boldsymbol{u}_{\min,i} \leq \boldsymbol{u}_i \leq \boldsymbol{u}_{\max,i}. \tag{5}$$

- Constraint on obstacle avoidance:

$$\|\boldsymbol{p} - \boldsymbol{p}_o\| \geq \max(r, \delta_{\text{wall}})\,. \tag{6}$$

Since ERG is an add-on constrained control scheme, it requires a pre-stabilized system [11]. Therefore, we first present the robot model and stabilizing control law, and then introduce the proposed ERG formulation.

4.1 Stabilizing control law

In this subsection, we present the nonlinear kinematic model and a stabilizing control law for a differential-drive mobile robot. The following assumptions are adopted.

Assumption 3. *The mobile robot is rigid and subject to nonholonomic constraints typical of differential-drive robots, with no lateral slip [12].*

Assumption 4. *The robot states are estimated using an Extended Kalman Filter (EKF) with intermittent observations [14].*

For mobile platforms that are controlled through commanded velocities, such as the robot considered in this work (see Figure. 1), and under Assumption (3), the differential-drive robot is described by the following kinematic model [12]:

$$\begin{bmatrix}\dot{x}\\ \dot{y}\\ \dot{\theta}\end{bmatrix} = \begin{bmatrix}\cos\theta\\ \sin\theta\\ 0\end{bmatrix} v + \begin{bmatrix}0\\ 0\\ 1\end{bmatrix}\omega = \begin{bmatrix}\cos\theta & 0\\ \sin\theta & 0\\ 0 & 1\end{bmatrix}\mathbf{u}, \tag{7}$$

where the robot configuration is described by its planar pose $\boldsymbol{q} = [x\ y\ \theta]^\top \in \mathbb{R}^3$, $\boldsymbol{p} = [x\ y]^\top \in \mathbb{R}^2$ denotes the planar position in the world frame $\mathcal{W}$, θ its orientation, and $u = [v\ \omega]^\top$ is the commanded velocity input.

Let the desired posture be $q_v = [x_v\ y_v\ \theta_v]^\top$. A convenient way is to formulate the problem in the polar coordinates [15] as follows

$$\rho = \sqrt{(x_v - x)^2 + (y_v - y)^2}, \tag{8}$$

$$\gamma = \text{Atan2}(y_v - y, x_v - x) - \theta_v, \tag{9}$$

$$\delta = \gamma + (\theta_v - \theta). \tag{10}$$

A well-stablished nonlinear control law is proposed to be used [15]. For readability, the proofs are also reported in the following proposition.

Proposition 1. *Consider the differential drive robot model* (7) *and let $q_v = [x_v\ y_v\ \theta_v]^\top$ denote the desired posture. Then, under the nonlinear feedback law*

$$v = k_1\,\rho\cos\gamma, \tag{11}$$

$$\omega = k_2\gamma + k_1\frac{\sin\gamma}{\gamma}\cos\gamma\,(\gamma + k_3\delta)\,, \tag{12}$$

with gains $k_1 > 0$, $k_2 > 0$, and $k_3 > 0$, the equilibrium is asymptotically stable.

Proof. The result follows from a classical Lyapunov analysis (see [15]), which is reported here for completeness. Consider the Lyapunov candidate

$$V = \frac{1}{2}\left(\rho^2 + \gamma^2 + k_3\delta^2\right), \tag{13}$$

Differentiating (13) along the closed-loop trajectories and substituting (11)–(12) yields

$$\dot{V} = -k_1\rho^2\cos^2\gamma - k_2\gamma^2 \leq 0. \tag{14}$$

Since $\dot{V}(t)$ is negative semi-definite, only stability can be concluded. However, using Barbalat lemma as shown in [15], the system is Asymptotically Stable (AS) for the equilibrium point. □

4.2 Governing unit

As discussed in the previous section, the ERG governing unit modifies the applied reference to ensure continuous satisfaction of the constraints. In this work, we adopt the trajectory-based ERG formulation [11]. The trajectory-based ERG updates the reference as the product of two components: the *Navigation Field* (NF) $\eta(q_v, r)$ and the *Dynamic Safety Margin* (DSM) $\Delta(q, \dot{q}, q_v)$.

The navigation field $\rho(q_v, r)$ defines a vector field that generates a desired steady-state admissible direction toward the reference goal. The DSM $\Delta(q, \dot{q}, q_v)$ is a scalar function that regulates the rate of change of the applied reference based on the distance between the predicted transient of the pre-stabilized system and the constraint boundaries. The DSM is strictly positive when all constraints are predicted to be satisfied over the future evolution starting from the current state q and $\dot{q}$, and it becomes zero when at least one constraint is violated.

The ERG update law is formally defined as

$$\dot{q}_v = \rho(q_v, r)\Delta(q, \dot{q}, q_v). \tag{15}$$

The following subsections provide a detailed description of the navigation field and the dynamic safety margin.

4.2.1 Navigation field

The navigation field can be designed in operational space using an attraction and repulsion field

$$\rho(q_v, r) = \rho^{att} + \rho^{rep}. \tag{16}$$

Let us consider the following attraction field

$$\rho^{att} = \frac{r - q_v}{\max(||r - q_v||, \eta)}, \tag{17}$$

where $\eta > 0$ is a smoothing parameter ensuring that the attraction field is a class C^1 function.

To ensure safe navigation in the presence of obstacles, a *repulsive field* is incorporated into the update law. It consists of two complementary components

$$\rho^{rep} = \rho^{rad} + \rho^{rot}. \tag{18}$$

The repulsion term acts exclusively on the positional part of the robot state. Let $p_v = [x_v \quad y_v]^\top$ and $p_o = [x_o \quad y_o]^\top$ denote respectively the robot and obstacle positions, and define $d = \|p_v - p_o\|$. The radial repulsive field is given by

$$\rho^{rad} = -\frac{p_v - p_o}{\|p_v - p_o\|} b(d, \epsilon), \tag{19}$$

where $b(d, \epsilon) : \mathbb{R} \to \mathbb{R}$ is the magnitude of the repulsion

$$b(d, \epsilon) = \max\left(\frac{\epsilon - d}{\epsilon - \delta}, 0\right), \tag{20}$$

where $\epsilon > 0$ is the influence margin and δ is the safety margin.

As reported in [16], radial repulsion can lead to *local minima* when it cancels the attractive field. To avoid convergence to such configurations, a *rotational (vortex) field* is introduced to generate an artificial field perpendicular to the line connecting the robot and the obstacle, encouraging the robot to move around the obstacle. The rotational component is defined as

$$\rho^{\text{rot}} = -\operatorname{sgn}(\alpha) \frac{b_{rot}(d, \epsilon^\star)}{\|p_v - p_o\|} \begin{bmatrix} -(y_v - y_o) \\ (x_v - x_o) \end{bmatrix}, \tag{21}$$

where α is the signed angle between the attractive field and the obstacle radial direction, defined following [16], and $\epsilon^\star \in (0, \epsilon)$ determines the activation region of the rotational field, and the activation function is

$$b_{rot}(d, \epsilon^\star) = \max\left(\frac{\epsilon^\star - d}{\epsilon^\star - \delta_m}, 0\right), \tag{22}$$

where δ_m denotes the distance at which radial-attractive cancellation occurs.

The two repulsive components act on non-overlapping intervals of the distance, therefore we have

$$\rho^{\text{rep}} = \begin{cases} \rho^{\text{rot}} & \text{if } d < \epsilon^\star, \\ \rho^{\text{rad}} & \text{if } \epsilon^\star \le d < \epsilon, \\ 0 & \text{if } d \ge \epsilon. \end{cases} \tag{23}$$

When (23) is active, the robot is first pushed away from the obstacle through a radial field and, when approaching the region where radial-attractive cancellation occurs, a tangential repulsion takes over. This mechanism ensures smooth and reliable navigation even in scenarios where classical artificial potential fields suffer from local minima.

4.2.2 Dynamic safety margin

First, we initialize the predicted state at the current time t as

$$\hat{q}_{t'=t} = q(t). \tag{24}$$

Since the considered mobile robot is velocity-controlled, the forward evolution required for the DSM computation is predicted using the kinematic model of the system

$$\begin{cases} \hat{q}_{t'+\Delta t} = \hat{q}_{t'} + \begin{bmatrix} \cos\hat{\theta}_{t'} & 0 \\ \sin\hat{\theta}_{t'} & 0 \\ 0 & 1 \end{bmatrix} \hat{u}_{t'}\, \Delta t, \\ \hat{u}_{t'} = u(\hat{q}_{t'}, q_v), \end{cases} \tag{25}$$

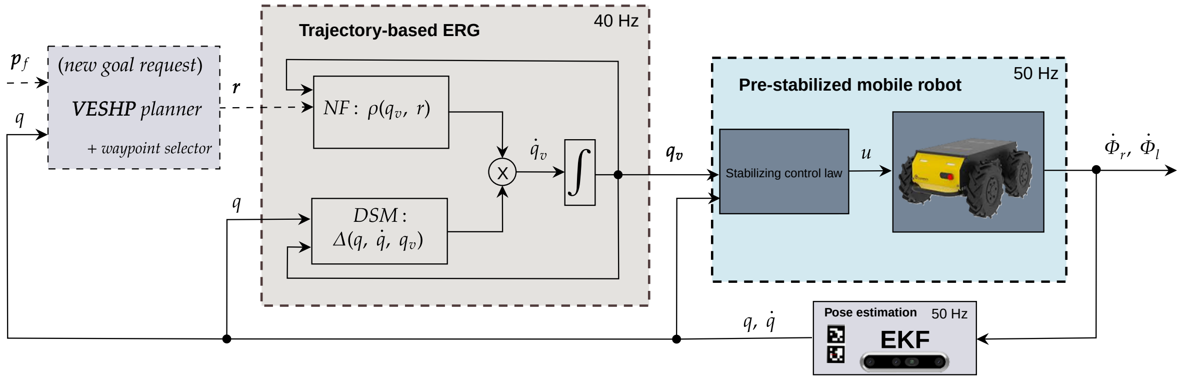

Figure 2. The proposed navigation framework. The mobile robot is pre-stabilized, and the applied position reference q_v is generated online by the ERG at 40 Hz. The VESHP planner computes a globally shortest geometric path given an initial position p_0 and a final position p_f and provides a finite sequence of waypoints p_i. A waypoint is selected and passed as a set-point reference to the ERG, which autonomously generates and executes a motion while enforcing constraints. The VESHP visibility graph is pre-computed offline based on the map of the environment, and shortest-path computation is triggered only when a new desired position is requested (online). The wheel velocities are denoted by $\dot{\phi}_r$ and $\dot{\phi}_l$. An EKF with intermittent observations is used to estimate the robot states q and $\dot{q}$.

with Δt the prediction sampling time.

The DSM on position is evaluated over the predicted motion. For each prediction step, the position p is compared against its admissible bounds $p_{\min}$ and $p_{\max}$:

$$\Delta p_{\min} = \min_{t\in[0,T]} \left\{p_{\text{pred},i} - (1+\delta_p)\, p_{\min,i}\right\}, \tag{24}$$

$$\Delta p_{\max} = \min_{t\in[0,T]} \left\{(1-\delta_p)\, p_{\max,i} - p_{\text{pred},i}\right\}, \tag{25}$$

with $\delta_p \in [0, 1]$. The position safety margin is

$$\Delta p = \min(\Delta p_{\min},\ \Delta p_{\max}). \tag{26}$$

Similarly for the inputs:

$$\Delta u_{\min} = \min_{t\in[0,T]} \left\{u(q_{\text{pred}}) - (1+\delta_u)\, u_{\min,i}\right\}, \tag{27}$$

$$\Delta u_{\max} = \min_{t\in[0,T]} \left\{(1-\delta_u)\, u_{\max,i} - u(q_{\text{pred}})\right\}, \tag{28}$$

and

$$\Delta_u = \min(\Delta u_{\min},\ \Delta u_{\max}). \tag{29}$$

The DSMs for obstacle avoidance of cylindrical obstacles, and polygonal obstacles are given as

$$\Delta p^{\text{cyl}}_{\text{obs}} = \min_{t\in[0,T]} \left(\|p_{\text{pred}} - p_o\| - r_j\right), \tag{30}$$

$$\Delta p^{\text{poly}}_{\text{obs}} = \min_{t\in[0,T]} \left(\|p_{\text{pred}} - p_o\| - \delta_{wall}\right), \tag{31}$$

Combining the two obstacle DSMs, yields

$$\Delta_{p_{obs}} = \min\{\Delta p^{\text{cyl}}_{\text{obs}},\ \Delta p^{\text{poly}}_{\text{obs}}\}. \tag{32}$$

Finally, the total DSM is

$$\Delta_T = \min\left(\kappa_p\, \Delta p,\ \kappa_u\, \Delta_u,\ \ \kappa_o\, \Delta p_{\text{obs}}\right), \tag{33}$$

where κ_q, κ_u, and κ_o are positive scaling coefficients.

5 Results

In this section, we report the results obtained with the proposed framework. Specifically, i) experimental results obtained with a mobile robot in a laboratory setting, and ii) numerical simulations conducted in a more complex construction-like environment. Simulations are used to complement the experimental results by investigating more complex scenarios that cannot be reproduced in the laboratory due to space constraints. Videos of the experiments are available as supplementary material [1].

For both cases, Assumption 2 is adopted, and a two-dimensional map of the environment is assumed to be available, either from Building Information Modeling (BIM) data or obtained through a prior mapping phase using onboard sensors such as LiDAR [17]. Based on this map, a global shortest path is computed using the VESHP algorithm and then through a waypoint selector is provided to the ERG for safe execution.

Throughout the experiments, the following controller gains are used $k_1 = 0.8$, $k_2 = 2.5$, and $k_3 = 3$. Position limits considered are $P_{\min} = [-10, -10]$ m and $P_{\max} = [10, 10]$ m, and the control input is $u = [v\ \omega]^\top$, with $v \in [-1, 1]$ m/s and $\omega \in [-2, 2]$ rad/s. The ERG parameters are $\eta = 0.005$, $\epsilon = 0.7$, $\epsilon^\star = 0.9$, $\kappa_p = 1.5$, $\kappa_u = 1$, $\kappa_o = 1$, with robustness margins $\delta_p = 0.1$ and $\delta_u = 0.1$.

[1] https://drive.google.com/drive/folders/1wc2hIBlPFVrUdD3QjWGsw3Mh2MVrDbK8?usp=sharing

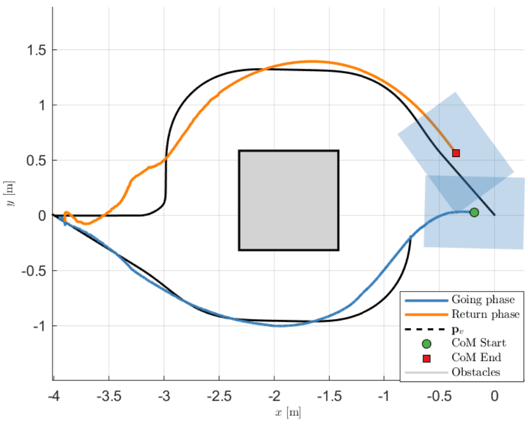

Figure 3. Trajectory of the system in x and y axes.

5.1 Experimental validation

Experimental validation is conducted using a Husky A200 differential-drive mobile robot. The robot pose is estimated using an intermittent Kalman filter [14], with measurements obtained from an Intel RealSense D456 camera operating at 60 fps, with AprilTags as visual markers.

Two representative scenarios are considered: i) avoidance of a single obstacle in a configuration that typically leads to a local minimum for standard ERG formulations [11], and ii) navigation in a laboratory environment with two obstacles.

In the first experiment (see, Figure 3), a cubic obstacle (0.9×0.9 m) is placed directly in front of the robot while the desired goal lies beyond it. This configuration is a typical local minima for conventional ERG, causing the robot to stop in front of the obstacle. As shown in Figures 3-4, the robot with the proposed ERG successfully reaches the goal $p_v = [-4, 0]^\top$ without getting stuck. After reaching the target, the reference is switched back to the initial position $p_v = p_0 = [0, 0]^\top$. Since only one obstacle is present, for this experiment we only use the ERG layer.

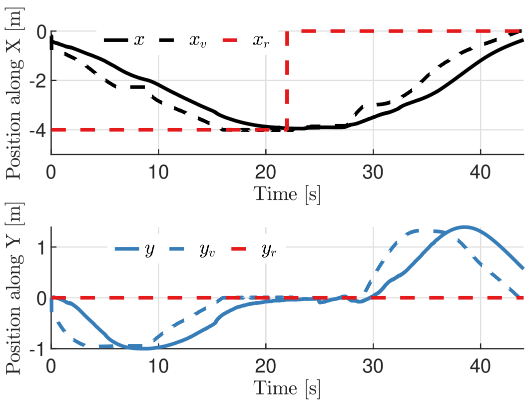

Figure 4. Position in x and y w.r.t. time.

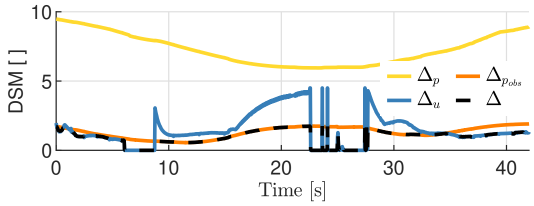

Figure 5. Dynamic safety margins (DSMs).

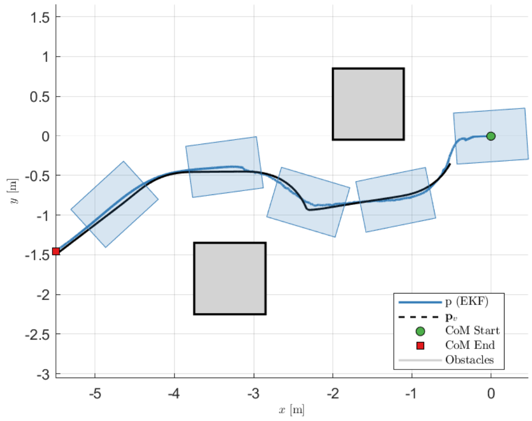

Figure 6. Trajectory of the system in x and y axes.

This behavior is achieved through the combined action of the radial ρ^{rad} and rotational ρ^{rot} components of the repulsive field, which continuously reshape the navigation field toward an admissible path around the obstacle. Figure 5 reports the evolution of the DSMs during the maneuver, showing that only the velocity constraint Δ_u becomes active (i.e., reaches zero) during the task. These results show that the ERG with the proposed repulsion field is capable of guiding the robot around obstacles while effectively avoiding local minima and satisfying the constraints.

In the second experiment (see Figure 1), two cubes and the walls are considered as obstacles, resulting in a more challenging navigation scenario to assess the proposed framework in the presence of multiple obstacles.

The mobile robot is assigned a desired position reference $p_v = [-5.5, -1.5]^\top$ that requires autonomous navigation across the obstacles. As shown in Figures 6-7, the proposed framework ensures executing a feasible path online, enabling the robot to avoid the obstacles and reach the destination while satisfying all constraints. The corresponding evolution of the DSMs is reported in Figure 8. Despite the increased complexity, the ERG successfully guides the robot around obstacles and toward the target.

5.2 Numerical simulation

Simulations are conducted in a planar environment with several static obstacles (Fig. 9). All obstacles are polyg-

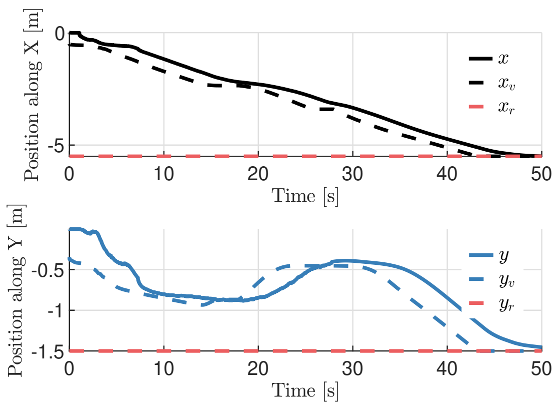

Figure 7. Position in x and y w.r.t. time.

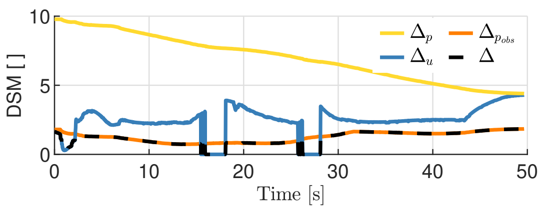

Figure 8. Dynamic safety margins.

onal except the cylindrical obstacle in orange, which is excluded from the VESHP planner and handled only by ERG, illustrating its ability to avoid unforeseen obstacles.

The blue points denote the VESHP waypoints and the red curve the robot trajectory under ERG control. VESHP computes a globally shortest path around known obstacles, while ERG drives the robot between waypoints enforcing collision avoidance and system constraints. When encountering the cylindrical obstacle, ERG locally deviates the robot before returning it to the VESHP path.

Table 1 compares the navigation strategies. ERG avoids collisions but yields longer paths, while PD leads to collisions and VESHP+PD produces shorter paths but fails with unmodelled obstacles. The proposed VESHP+ERG framework combines both advantages, providing global guidance through VESHP and safe execution through ERG while avoiding all the obstacles.

6 Conclusion

This paper presented a navigation framework for mobile robots in cluttered construction environments that combines global shortest-path planning with real-time constraint control. The VESHP planner provides globally optimal waypoints, while the ERG ensures continuous satisfaction of state, input, and collision-avoidance constraints during execution. Simulation and experimental results show that the proposed VESHP–ERG framework enables safe, efficient navigation while avoiding local minima.

Acknowledgements

This work was supported by the Research Foundation - Flanders (FWO) through the PhD fellowship grant numbers 1SHBX24N, 1S47925N, and by Innoviris and FARI (BrickieBots 2.0), and by the research program Artificiele Intelligentie Vlaanderen from the Flemish Government.

References

[1] Zemerart Asani, Michele Ambrosino, Bram Vanderborght, and Emanuele Garone. Towards safer and more efficient construction-the development of a multi-robotic system for heavy block assembly. In *2024 IEEE International Conference on Robotics and Automation (ICRA)*, pages 13–16. The International Association for Automation and Robotics in Construction, 2024.

[2] Zemerart Asani, Marco M Nicotra, and Emanuele Garone. Virtual mass tuning of overhead cranes. *IEEE Control Systems Letters*, 2025.

[3] Lingdong Zeng, Shuai Guo, Jing Wu, and Bernd Markert. Autonomous mobile construction robots in built environment: A comprehensive review. *Developments in the Built Environment*, 19:100484, 2024.

[4] Zemerart Asani, Michele Ambrosino, Andres Cotorruelo, and Emanuele Garone. Nonlinear model predictive control of a 5-dofs boom crane. In *2021 29th Mediterranean Conference on Control and Automation (MED)*, pages 867–871. IEEE, 2021.

[5] Zemerart Asani, Michele Ambrosino, Bram Vanderborght, and Emanuele Garone. Implementation of a heterogeneous multi-robot system for a construction task. *IFAC-PapersOnLine*, 56(2):3373–3378, 2023.

[6] Liangcheng Yu, Merit M Huang, Suwen Jiang, Chen Wang, and Mabao Wu. Unmanned aircraft path planning for construction safety inspections. *Automation in Construction*, 154:105005, 2023.

[7] Guang Yang, Shuoyu Wang, Hajime Okamura, Bo Shen, Yasuhiro Ueda, Toshiaki Yasui, Tetsuya Yamada, Yuki Miyazawa, Satomi Yoshida, Yuta Inada, et al. Hallway exploration-inspired guidance: applications in autonomous material transportation in construction sites. *Automation in Construction*, 128:103758, 2021.

[8] Zeli Wang, Heng Li, and Xiaoling Zhang. Construction waste recycling robot for nails and screws: Computer vision technology and neural network approach. *Automation in Construction*, 97:220–228, 2019.

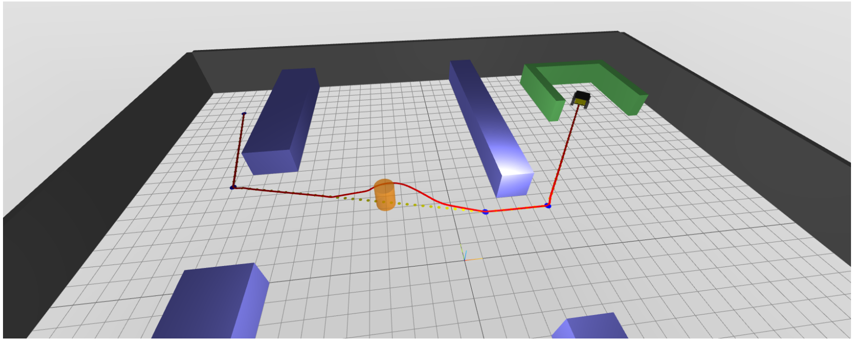

(a) Isometric zoom on the robot trajectory

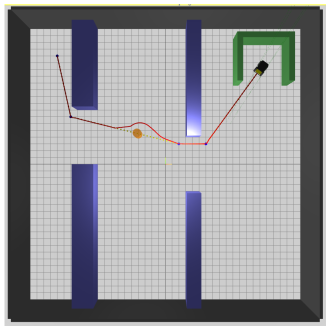

(b) Top view of the full scene with the robot trajectory.

Figure 9. Robot navigation in a cluttered construction environment using the VESHP–ERG framework. The global VESHP planner considers only the polygonal obstacles (shown in blue, green, and black) and generates a sequence of goal points, indicated by the blue dots. The ERG-based control layer accounts for all obstacles, including the cylindrical obstacle (orange) that is not considered during global planning. The red curve represents the trajectory executed by the mobile robot, which safely navigates between the VESHP waypoints while avoiding all obstacles and reaching the final goal.

Table 1. Comparison of navigation strategies. The * correspond to the scenario with an unmodelled obstacle.

Method	Path (m)	Time (s)	Collision	Path* (m)	Time* (s)	Collision*
PD	15.529	18	Y	15.529	18	Y
VESHP+PD	21.937	30	N	21.934	31	Y
ERG	25.162	48	N	25.876	75	N
VESHP+ERG	21.549	43	N	22.455	70	N

[9] Xiaotian Ye, Hongling Guo, Ziyang Guo, and Zhubang Luo. A construction robot path planning method based on safe space and worker trajectory prediction. In *ISARC. Proceedings of the International Symposium on Automation and Robotics in Construction*, volume 41, pages 227–235. IAARC Publications, 2024.

[10] Ouassim Benhamouche, Zemerart Asani, Andrés Cotorruelo, Benjamin Wauthion, Bram Vanderborght, and Emanuele Garone. On an almost closed-form fast generation of euclidean shortest path trajectories in cluttered environments. In *2025 11th International Conference on Automation, Robotics, and Applications (ICARA)*, pages 399–403. IEEE, 2025.

[11] Kelly Merckaert, Bryan Convens, Marco M Nicotra, and Bram Vanderborght. Real-time constraint-based planning and control of robotic manipulators for safe human–robot collaboration. *Robotics and Computer-Integrated Manufacturing*, 87:102711, 2024.

[12] Mohamed W Mehrez, George KI Mann, and Raymond G Gosine. Comparison of stabilizing nmpc designs for wheeled mobile robots: An experimental study. In *2015 Moratuwa Engineering Research Conference (MERCon)*, pages 130–135. IEEE, 2015.

[13] Johannes Köhler, Daniel Zhang, Raffaele Soloperto, Andrea Carron, and Melanie Zeilinger. An mpc framework for efficient navigation of mobile robots in cluttered environments. *arXiv preprint arXiv:2509.15917*, 2025.

[14] Bruno Sinopoli, Luca Schenato, Massimo Franceschetti, Kameshwar Poolla, Michael I Jordan, and Shankar S Sastry. Kalman filtering with intermittent observations. *IEEE transactions on Automatic Control*, 49(9):1453–1464, 2004.

[15] Bruno Siciliano, Lorenzo Sciavicco, Luigi Villani, and Giuseppe Oriolo. *Robotics: modelling, planning and control*. Springer, 2009.

[16] Roberto Ancona. Redundancy modelling and resolution for robotic mobile manipulators: a general approach. *Advanced robotics*, 31(13):706–715, 2017.

[17] Jörg Husemann, Maximilian Kunz, Marcel Suiker, and Karsten Berns. From bim to autonomous navigation: Using bim models to enable autonomous navigation and localization in construction environments. July 2025. doi:10.22260/ISARC2025/0020.